

# GridInSight: Monitoring Electricity Using Visible Lights

Zeal Shah, Alex Yen, Ajey Pandey, and Jay Taneja  
{zshah, ayen, apandey, jtaneja}@umass.edu  
STIMA Lab, Department of Electrical and Computer Engineering  
University of Massachusetts, Amherst

## ABSTRACT

We demonstrate *GridInSight*, a suite of techniques that leverage low-cost, non-intrusive, and commodity smartphone and machine vision cameras to measure electricity grids. Specifically, we develop techniques to measure electricity grid frequency, phase (indoors), and phase (outdoors) across a mix of cameras with errors of 1-2%, 2-5%, and 3-10%, respectively. Further, we develop a novel technique and show an error of 8-15% for measuring voltage on a lightbulb that our system had not seen previously. The ability to cheaply and pervasively measure power quality with non-intrusive, off-the-shelf hardware can enable a wide range of applications for monitoring electricity grids, particularly in emerging economies.

### ACM Reference Format:

Zeal Shah, Alex Yen, Ajey Pandey, and Jay Taneja. 2019. GridInSight: Monitoring Electricity Using Visible Lights. In *The 6th ACM International Conference on Systems for Energy-Efficient Buildings, Cities, and Transportation (BuildSys '19)*, November 13–14, 2019, New York, NY, USA. ACM, New York, NY, USA, 10 pages. <https://doi.org/10.1145/3360322.3360855>

## 1 INTRODUCTION

A network of millions of interconnected sources and consumers delivering its goods at light speed with few if any warehouses for inventory – the electricity grid remains as one of humanity’s foremost engineering marvels. The most visible evidence of the ubiquity of the grid are the billions of artificial lights that surround our indoor and outdoor lives. In addition to illumination, lights provide more than meets the eye – the intricate patterns of light flicker caused by the cycling of alternating current electricity can expose insights into the dynamics of electricity grid operation. Increasingly smaller, cheaper, more capable, and more pervasive imaging technology – found on commodity smartphones and vision cameras – can help to capture these subtle variations in light.

At the same time, many grids and utilities are unprepared for the oncoming tsunami of change wrought by the democratization of electricity infrastructure, largely driven by inexorable reductions in the cost of renewables and storage. Electricity grids, particularly those in emerging regions, typically suffer from a dearth of sensing; without enough information about the status of the grid and the quality of the electricity at endpoints, utilities struggle to provision electricity reliably and customers struggle to thrive. Traditional

methods of grid observation – smart meters or in-network sensors like phasor measurement units and the analytics systems needed to harness their data – are often out of reach, too expensive and not economical at scale.

In this paper, we explore the potential to measure electricity grid characteristics using non-intrusive photography. We build on previous work [3, 25] that uncovered the link between light patterns and grid conditions. We introduce *GridInSight*, a suite of techniques that leverage low-cost, non-intrusive, and commodity imaging devices to measure electricity grids. Our work develops techniques and evaluates the capability of cameras to measure power quality and grid dynamics. Specifically, our novel contributions include:

- A database characterizing the bulb response functions (BRFs) of 74 lightbulbs on a 60 Hz supply
- A comparison of techniques for empirical measurement of electricity grid frequency solely from camera images of lightbulbs
- A first-of-its-kind technique for measuring electricity grid voltage purely using camera images of lightbulbs
- Comparative evaluation of two smartphone cameras and a machine vision camera for measurement of grid parameters, including detailed error measurements

The paper begins with a survey of related work on power quality monitoring before providing background on the core concepts of lighting with alternating current supply and the rolling shutter photographic effect. Sections 4, 5, and 6 introduce our methodology for measuring grid frequency, phase, and voltage using camera images, followed by implementation details in Section 7. We then provide experimental results for each of the measurement parameters in Section 8 and conclude with discussion and future work.

## 2 RELATED WORK

Power quality monitoring is important for utilities to improve the efficiency of their systems and to reduce financial losses [23]. Using data recorded by a monitoring system, utilities can plan the maintenance of distribution grid equipment and take necessary measures to reduce power quality disturbances [23]. User appliances and equipment are directly affected by the quality of power being delivered to their homes and offices [13] and so power quality monitoring systems can also help utilities make their system safer for end users [23]. Advanced metering infrastructure has been the conventional choice for voltage quality and frequency monitoring purposes [2, 13, 14, 18, 19]. Additionally, to address the voltage imbalance problem caused due to uneven loading of phases of the distribution network, researchers have demonstrated the use of smart meter data to detect phases to supplement distribution-level phase balancing studies [16]. However, smart metering infrastructure can be expensive [13]. We propose an affordable and non-intrusive

---

Permission to make digital or hard copies of all or part of this work for personal or classroom use is granted without fee provided that copies are not made or distributed for profit or commercial advantage and that copies bear this notice and the full citation on the first page. Copyrights for components of this work owned by others than ACM must be honored. Abstracting with credit is permitted. To copy otherwise, or republish, to post on servers or to redistribute to lists, requires prior specific permission and/or a fee. Request permissions from [permissions@acm.org](mailto:permissions@acm.org).

*BuildSys '19*, November 13–14, 2019, New York, NY, USA

© 2019 Association for Computing Machinery.

ACM ISBN 978-1-4503-7005-9/19/11...\$15.00

<https://doi.org/10.1145/3360322.3360855>

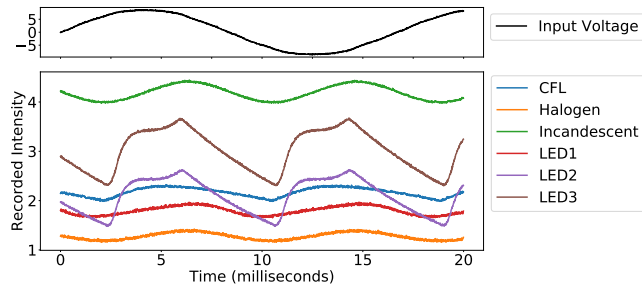


**Figure 1: Bulb Response Functions of different bulbs recorded using a photo-transistor. Distance between bulbs and transistor was held constant at 40cm. Recording was triggered at the zero-crossing of input AC voltage wave.**

system for monitoring voltage and frequency as well as detecting phases at distribution level.

Voltage, frequency, and phase of the supply affect the intensity and flickering pattern of artificial lighting [24]. This allows bulb characteristics like intensity and flicker pattern to serve as a side channel about the grid powering the bulb. Sheinin et al. [24] developed a novel coded exposure imaging system for passively sensing the bulb’s response to obtain the underlying electric phase information but it required tethering to the AC grid which makes it intrusive. Other researchers have also demonstrated non-intrusive monitoring of a grid using imaging through cameras and other techniques. Bianco et al. [3] used hypertemporal imaging to observe grid phases of light sources across the NYC skyline by employing a digital camera and a special liquid crystal shutter. Breda et al. [4] used a cell phone microphone and a fan to sense grid voltage. Sheinin et al. [25] demonstrated that off-the-shelf cameras can be used for grid sensing by exploiting the rolling shutter mechanism of digital cameras. The rolling shutter mechanism has been modeled and analyzed in multiple research papers [10, 15] and has been used for a variety of sensing purposes, including sensing grid frequency fluctuations in indoor lighting [8, 26], measuring principal frequency components of vibrations of man-made objects like motors [28], calculating pose and velocity of rigid objects [1], and developing a mechanism for communication between cameras and displays while in the process of capturing photos which used rolling shutter cameras as receivers [12].

Smartphones are easily available and increasingly affordable, and most smartphone cameras have rolling shutter sensors. In this research, we use the concepts presented in previous work [24, 25] to record bulb responses and detect phases using the rolling shutter mechanism of smartphone cameras. Additionally we propose methods to passively monitor frequency, phase, and voltage of the grid. We also compare the measurement accuracy of smartphones and vision cameras.

## 3 BACKGROUND

### 3.1 AC Lighting

Electricity is delivered to the end consumer in three phases. Each consumer can be tapped on to a single phase or the full 3-phase connection based on a consumer’s power requirements. In 3-phase

configuration, AC waves in each phase wire are shifted by  $120^\circ$  from AC waves in another. If we consider one phase connection to be at  $0^\circ$  then the other two connections of a 3-phase system will be at  $120^\circ$  and  $240^\circ$ . AC voltage wave is represented as  $V(t) = V_{max} \sin(2\pi ft - \phi)$  where  $\phi$  is the phase of the wave,  $f$  is frequency (50Hz or 60Hz), and  $V_{max}$  is the maximum voltage amplitude (120V or 230V). Let us assume that we connect one bulb to every phase of a 3-phase system. In every phase connection, the voltage pulsates at a frequency  $f$  and so the bulb’s output will also pulsate. Bulbs will flicker at a frequency double the AC supply frequency, *i.e.* at  $2f$ [24]. For this paper, we define  $\Delta = 1/2f$  as duration of a bulb’s flicker cycle. The phase difference between the bulbs will cause their flickering patterns to be shifted in time from one another. Flickering of light bulbs is also governed by their make and internal circuits [25].

In previous work [24, 25], the bulb’s temporal flickering behavior as related to input voltage is introduced as a unit-less Bulb Response Function (BRF). The BRF value at a time  $t$  is defined as the ratio of intensity measured to the temporal average of measured intensity. The BRF can be acquired by recording timely measurements from a photo-diode placed near a bulb [24]. Using the suggested methodology, we created a database of BRFs of different bulbs as a part of this research which is discussed in more detail in Section 7.3. Every bulb has its own characteristic BRF as shown in Figure 1. Alternatively, a BRF can be defined as a bulb response wave which is a function of time and phase of the AC supply, and can be denoted as  $B_\beta(t - \phi_s \frac{\Delta}{2\pi})$ , where  $\beta$  denotes bulb type,  $t$  is time,  $\phi_s$  is the phase of AC supply [25]. Employing this new definition for a bulb’s response, one can sense a BRF using imaging. If  $M$  light sources are illuminating an object, the captured intensity of the object can be mapped to image pixel response as follows

$$i(r, c, t) = \sum_{s=1}^M \tau_s(r, c) B_s(t - \phi_s \frac{\Delta}{2\pi}) \quad (1)$$

where,  $(r, c)$  denotes (row, column) pair to index an image pixel. Sheinin et al. [25] defines  $\tau_s(r, c)$  as a response of an image pixel to actual illumination by a source  $s$  and terms it as the light transport coefficient at the given pixel corresponding to a source  $s$ .  $\tau_s(r, c)$  forms a matrix of  $r$  rows and  $c$  columns for the complete image. According to Sheinin et al. [25],  $\tau_s(r, c)$  contains information associated with image radiance which is dependent on factors like lens aperture, distance of source from camera, exposure duration, and more.

### 3.2 Rolling Shutter Camera

In this subsection, we introduce a method developed by Sheinin et al. [25] for leveraging the rolling shutter effect in digital cameras to measure electrical grid activity from photographs. A majority of modern smartphone and DSLR cameras are rolling shutter cameras. In a rolling shutter camera, every row of the sensor is exposed after a delay  $D$  relative to the preceding row [15, 21, 25].  $D$  depends on the make of a camera’s sensor. If the topmost row of the sensor was exposed at time  $t_0$ , then the  $r^{th}$  row will be exposed at time  $t_0 + rD$ . Every row will be exposed for time equal to the exposure time ( $T_{exp}$ ) set using the shutter speed setting of the camera. Thus, a rolling shutter camera provides a temporal sampling rate of  $1/D$

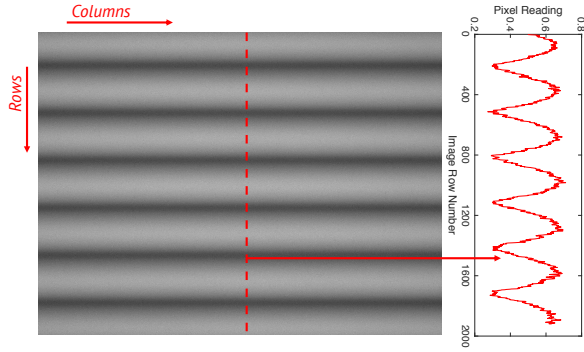


**Figure 2: Image of a wall illuminated by a bulb captured using an IDS vision camera at 1.25ms shutter speed. The dashed vertical line of pixels represents the flicker wave pattern of the bulb (as seen on the right).**

Hz. Substituting the value of  $t$  in Equation (1), we get

$$i_{roll}(r, c) = \sum_{s=1}^M \tau_s(r, c) B_s(t_0 + rD - \phi_s \frac{\Delta}{2\pi}) \quad (2)$$

When a scene illuminated by AC lighting is captured using a rolling shutter camera, we obtain a vertical spatial pattern with a period of  $\Delta/D$  rows, *i.e.* a spatial frequency of  $D/\Delta$  as shown in Figure 2. The flicker wave pattern of a bulb can be obtained by extracting a column of pixels from the image region dominated by that specific bulb as shown in Figure 2. Furthermore, when the exposure time  $T_{exp}$  is set to  $\Delta$  or an integer multiple of it, the image becomes invariant to the BRF of sources illuminating the scene [25]. In other words, the image behaves as if captured under DC illumination [25].

$$i_{dc}(r, c) = \sum_{s=1}^M \tau_s(r, c) \quad (3)$$

For an image region dominated by a single source  $s'$  [25],

$$i_{dc}(r, c) = \tau_{s'}(r, c) + \sum_{s \neq s'} \tau_s(r, c) \approx \tau_{s'}(r, c) \quad (4)$$

Therefore, for an image region dominated by a single source  $s'$  the image intensity signal can be given as [25],

$$i_{roll}(r, c) = i_{dc}(r, c) B_{s'}(t_0 + rD - \phi_{s'} \frac{\Delta}{2\pi}) \quad (5)$$

Equation (5) denotes that we can obtain the BRF of source  $s'$  by extracting a column of pixels from the normalized image ( $\frac{i_{roll}(r, c)}{i_{dc}(r, c)}$ ) of the region dominated by source  $s'$ . This concept plays a major role in frequency and phase calculations that will be discussed in Sections 4 and 5. Thus, for frequency and phase detection experiments, we capture two different kinds of images – a rolling image and a DC image. The rolling image is an image captured at a shutter speed of less than  $1/2f$  seconds. The DC image is captured at a shutter speed equal to or an integer multiple of  $\Delta (=1/2f)$  seconds.

## 4 FREQUENCY MONITORING

Capturing a bulb's response can provide us with insights into frequency of the AC supply powering the bulb. We record a bulb's response function by capturing a rolling image and a DC image of a surface being illuminated by that bulb. Dividing the rolling image with its DC counterpart will remove scene-dependent information from the resulting image [25]. As discussed in Section , an image recorded using a rolling shutter sensor possesses a vertical spatial pattern, and every row of the image will correspond to a timestamp. We extract and plot a column of pixels and convert the row numbers to timestamps by multiplying every row number with the inter-row delay value  $D$  as shown in Figure 3(a). In this section, we discuss three different techniques to calculate frequency of the AC supply using the extracted signal  $S(t)$ .

### 4.1 Finding Peaks

In this approach, we filter the signal  $S(t)$  to make it smooth and then locate its peaks as shown in Figure 3(b). Let us assume the recorded signal has  $n$  peaks ( $p_1, p_2, p_3, \dots, p_n$ ) and each peak corresponds to a time value ( $t_1, t_2, t_3, \dots, t_n$ ). The period  $P$  of the signal can be calculated as an average of time differences between consecutive peaks.

$$P = \frac{\sum(t_2 - t_1) + (t_3 - t_2) + \dots + (t_n - t_{n-1})}{n - 1} \text{seconds} \quad (6)$$

Frequency ( $f$ ) of the AC supply can then be calculated using

$$f = \frac{1}{P} \times 0.5 \text{Hz} \quad (7)$$

### 4.2 Power Spectral Density

In this approach, we first obtain the strength of different frequency components of signal  $S(t)$  by estimating its power spectrum. We implement Welch's method to estimate the power spectral density (PSD) of the signal which basically splits the time signal into overlapping blocks, creates a periodogram for each block, and then takes an average of all the periodograms [11]. As a result, we obtain a dataset containing a series of power-frequency pairs. The plot of power spectral density versus frequency for  $S(t)$  is shown in Figure 3(c). Frequency corresponding to the maximum power spectral density value is the frequency of signal  $S(t)$ , the frequency of bulb flicker. Therefore, the AC supply frequency is half the frequency value of bulb flicker.

### 4.3 Sine-Wave Fitting

The third technique for frequency monitoring is fitting a sine wave to the recorded signal  $S(t)$  as shown in Figure 3(d). The sine wave model used for fitting can be represented as follows:

$$h(t) = a \sin(bt + c) \quad (8)$$

Once the sine model is fit to the data, we obtain the values of coefficients  $a$ ,  $b$ , and  $c$ . Using the coefficient values, the AC supply's frequency can be calculated as:

$$f = \frac{b}{2\pi} \times \frac{1}{2} \text{Hz} \quad (9)$$

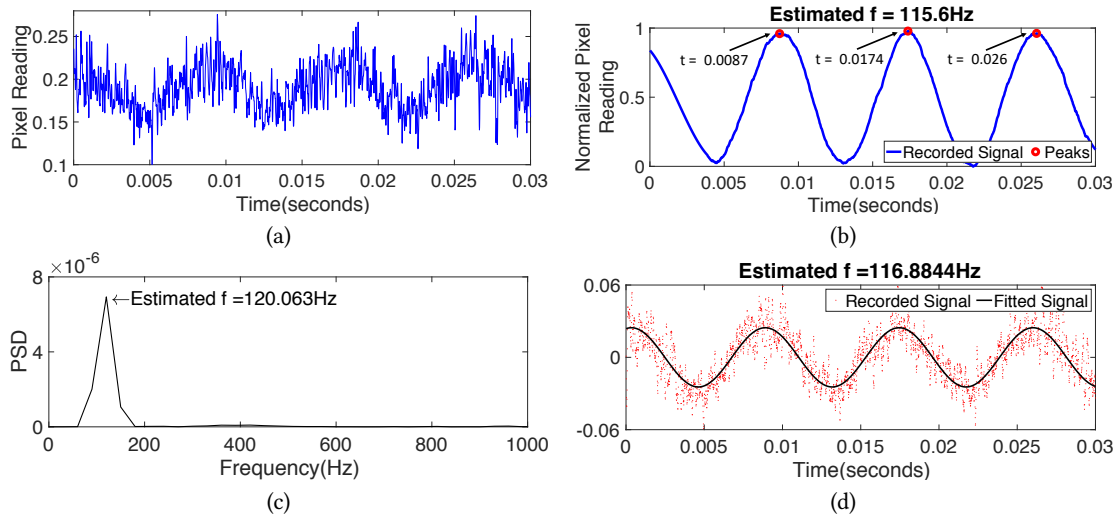


**Figure 3:** (a) A bulb's flicker waveform recorded using a One Plus 6 smartphone camera. (b) Detected peaks of the flicker waveform after passing it through a moving average filter. (c) Power spectral density of the signal plotted against frequency components. (d) A sine-wave fitted onto the recorded signal. Estimated frequency of bulb flicker has been shown in (b), (c), and (d).

## 5 PHASE DETECTION

Phase detection techniques discussed in this section can be used indoors and outdoors. Electric phases are a relative concept. This necessitates the fact that in order to detect phases, at least two light sources should be involved in the experiment. One of the light sources is assumed to be connected to the reference outlet. Phases associated with the remaining light sources are then calculated relative to the reference source.

### 5.1 Phase Detection for Indoor Scenes

We capture a rolling image ( $I_{roll}$ ) and a DC image ( $I_{dc}$ ) of a wall illuminated by two light sources ( $b1$  and  $b2$ ) - bulb1 and bulb2 as shown in Figure 4. Each light source is connected to a different phase outlet. The rolling image is then normalized by the DC image to improve bulb information recovery as suggested in [25]. The resultant normalized image ( $I_{norm}$ ) can be given as:

$$I_{norm}(r, c) = \frac{I_{roll}(r, c)}{I_{dc}(r, c)} \quad (10)$$

The resultant image contains two spatial vertical flicker wave patterns - one corresponding to each source as shown in Figure 4. The visible vertical spatial shift between the two flicker wave patterns denotes the phase difference between the two light sources. Let us extract a column of pixels from the regions dominated by each bulb in the resultant image ( $I_{norm}$ ) and denote columns as  $c1$  and  $c2$ . The column intensities can be represented as functions of row number ( $r$ ):  $i_{b1}(r)$  and  $i_{b2}(r)$ .

$$i_{b1}(r) = I_{norm}(r, c1) \quad (11)$$

$$i_{b2}(r) = I_{norm}(r, c2) \quad (12)$$

Here,  $r$  ranges from 1 to  $n$ , and  $n$  is the total number of rows in the captured image. We then normalize the signals using their

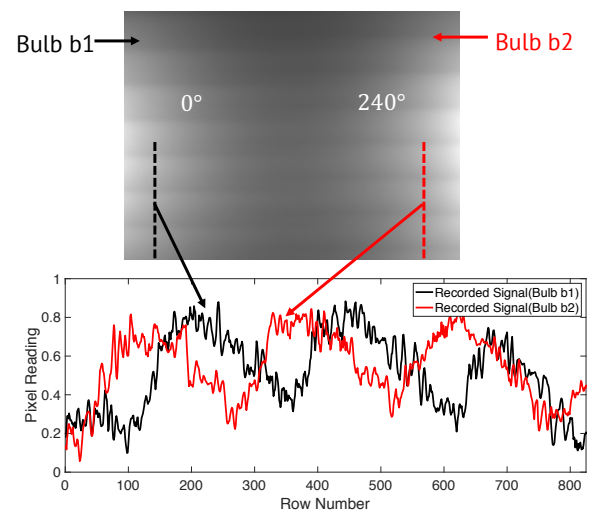


**Figure 4:** Image of a wall illuminated by two different CFL bulbs connected to power outlets  $240^\circ$  out of phase captured using an IDS vision camera. Flicker signals are extracted from regions dominated by each bulb. The extracted signals are shifted in space and time due to the phase difference between the sources.

respective mean intensity values as given in Equations (13, 14, 15).

$$mean_{b_j} = \frac{\sum_{r=1}^{r=n} I_{norm}(r, c_j)}{n} \quad (13)$$

$$i_{b1}^{norm} = \frac{i_{b1}(r)}{mean_{b1}} \quad (14)$$

$$i_{b2}^{norm} = \frac{i_{b2}(r)}{mean_{b2}} \quad (15)$$

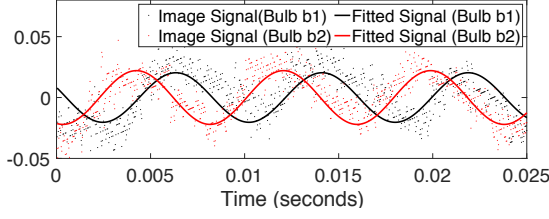


**Figure 5: Sine waves fitted to the two extracted flicker waveforms. The magnitude of time shift is equal to 2.9ms which gives a phase difference value of  $-125^\circ$  i.e., bulb b2 is connected to  $235^\circ$  phase relative to b1.**

Row numbers can be converted to timestamps by multiplying row number by inter-row delay  $D$ . This gives us two time-dependent flicker wave signals  $i_{b1}^{norm}(t)$  and  $i_{b2}^{norm}(t)$ . The signals  $i_{b1}^{norm}(t)$  and  $i_{b2}^{norm}(t)$  are shifted in time. This time shift ( $t_{shift}$ ) value can be used to calculate the phase difference using:

$$\phi = \frac{2\pi(t_{shift})}{\Delta} \quad (16)$$

where,  $\Delta$  represents the bulb flicker cycle period which is equal to  $\frac{1}{2f}$  and  $f$  is the AC supply frequency. In this section, we discuss two different techniques to measure the time shift value.

### 5.1.1 Sine-Wave Fitting.

In the first technique, the result of which is shown in Figure 5, we fit a sine wave individually to both the time signals. With two sine waves  $h_{b1}(t)$  and  $h_{b2}(t)$ , the time shift value between the waves can be calculated by finding the minimum time difference value between two signals. Since the concept of phases is relative, let us assume that bulb  $b1$  is connected to phase  $0^\circ$ . Using  $h_{b1}(t)$  as a reference, we shift  $h_{b2}(t)$  horizontally along the time axis until the difference between both the waves is minimum.

$$t_{shift} = \pm \operatorname{argmin}_t |h_{b1}(t) - h_{b2}(t)|^2 \quad (17)$$

(+/-) sign for time shift value is dictated by the position of shifted wave relative to the reference wave, i.e. leading or lagging. Once the time shift value is obtained, it is plugged into Equation (16) to get the phase difference value. Note that the sine fitting technique does not depend on the bulb type and its BRF.

### 5.1.2 BRF-Signal Fitting.

BRF-Signal fitting technique for time shift calculation was proposed in [25], and is dependent on the assumption that we know the bulb types and possess their respective BRFs beforehand. The time shift between the recorded signal and its corresponding BRF is calculated first. We implement least squares fitting to obtain the time shift for which the BRF best fits its corresponding recorded signal as shown in Figure 6.

$$t_s^{b1} = \pm \operatorname{argmin}_t |i_{b1}^{norm}(t) - \operatorname{BRF}_{b1}(t)|^2 \quad (18)$$

$$t_s^{b2} = \pm \operatorname{argmin}_t |i_{b2}^{norm}(t) - \operatorname{BRF}_{b2}(t)|^2 \quad (19)$$

The (+/-) sign for the time shift value is dictated by the position of shifted BRF wave relative to the reference wave, i.e. leading or lagging. Since we have assumed that the first bulb is connected

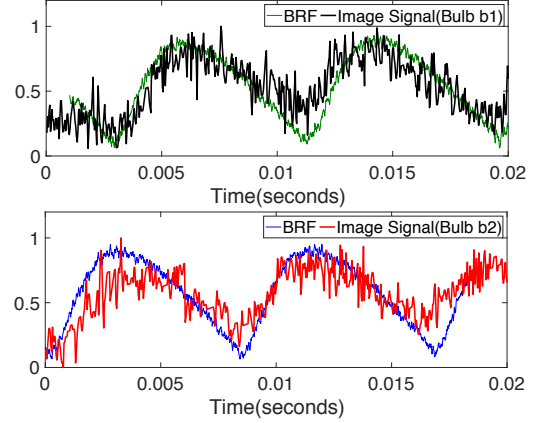


**Figure 6: Recorded image signals best-fitted with corresponding BRFs. The overall time shift magnitude is 2.69ms resulting in a phase difference value of  $-116^\circ$ , i.e. the phase angle associated with bulb b2 is  $244^\circ$  relative to bulb b1.**

to the reference outlet, the overall time shift value can then be calculated as a difference of individual Signal-BRF time shift values.

$$t_{shift} = t_s^{b1} - t_s^{b2} \quad (20)$$

We substitute the  $t_{shift}$  value in equation (16) to obtain the phase difference between the two bulbs.

## 5.2 Phase Detection for Outdoor Scenes

In the majority of outdoor scenes, it is almost impossible to see and record the flicker wave pattern as shown in Figure 7(a). It is also important to observe that in the outdoor scenes, the emitters are usually directly visible. For phase detection in such scenarios, we resort to two different methods as suggested in Sheinin et al. [25]. First, defocusing the lens blurs the scene and induces a point spread function around every light source in the frame. The point spread function of a source contains the flicker wave pattern of that source as shown in Figure 7(b). Defocusing can be helpful in scenes where the emitters are widely-spaced such that their point spread functions do not completely superimpose one another.

In the second technique, we induce the flicker pattern by using a 4-point star filter. The star filter is placed over the lens of the camera and aligned with the sensor such that a clear point spread function is observed around the light sources as shown in Figure 7(c). A vertical streak of light around the sources contains the flicker wave pattern of the light source.

Once we have the flicker wave pattern induced using either technique, the phase values can be calculated using the techniques discussed in Section 5.1.

## 6 VOLTAGE MONITORING

Image intensity is affected by two factors: (1) the intensity of a bulb illuminating the object being captured and (2) the distance between the camera and the object. Intensity of a bulb is dependent on input AC voltage and bulb type. To better understand the correlation between voltage, image intensity, and distance - we captured images of a wall illuminated by a bulb at different source voltage values

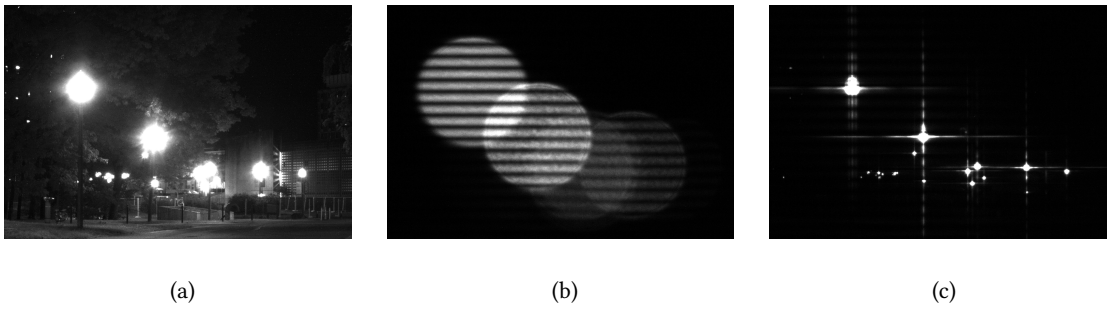


Figure 7: (a) Outdoor scene with directly visible emitters captured using the IDS vision camera. (b) Flicker patterns induced by lens defocusing. (c) Flicker patterns induced using a star filter on the lens.

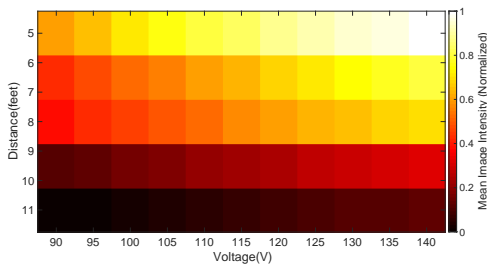


Figure 8: Heat map demonstrating variation in image intensity with change in voltage across the source and distance between the illuminated wall and camera. Uses a Philips CFL 26W bulb and IDS vision camera.

---

#### Algorithm 1 Regression Level 1

---

```

1: for every  $v$  in  $V$  do
2:   for every  $d$  in  $D$  do
3:      $i(d, v) = \text{mean}(I(d, v))$ 
4:   Curve Fitting Level 1 :  $i(D, v) = \frac{x_v}{D^2} + y_v$ 
5:   for every  $d$  in  $D$  do
6:      $\text{mult}(d, v) = \frac{i(d, v)}{i(d=1, v)}$ 
7:     # Since  $\text{mult}(d, v_1) \approx \text{mult}(d, v_2) \approx \dots \approx \text{mult}(d, v_n)$ , we calculate mean intensity multipliers for every distance value as:
8:     for every  $d$  in  $D$  do
9:        $\text{mult}(d) = \frac{\sum_{v \in V} \text{mult}(d, v)}{n}$ 
10:    return  $\text{mult}(D) = \{\text{mult}(d_1), \text{mult}(d_2), \dots, \text{mult}(d_m)\}$ 

```

---



---

#### Algorithm 2 Regression Level 2

---

**Require:**  $\text{mult}(D)$  array, and images  $I(d, v)$

```

1: Flatten each  $I(d, v)$  to a column vector  $IC(d, v)$ 
   # Make intensity (IC) independent of distance:
2: for every  $v$  in  $V$  do
3:   for every  $d$  in  $D$  do
4:      $IC(d, v) = \frac{IC(d, v)}{\text{mult}(d)}$ 
5: Curve Fitting Level 2 :  $\text{volt} = h \times IC + q$ 
6: return prediction_model

```

---

and distances, and the experiment was repeated for different bulbs. Results from one experiment are visualized in Figure 8. It was

observed that voltage ( $V$ ) and mean image intensity ( $I$ ) are directly related ( $V \propto I$ ), for a given distance ( $d$ ). Also, given the voltage, mean image intensity and distance are inversely related ( $I \propto 1/d$ ). These two relations were then used to build a per-bulb two-level regression model for voltage monitoring.

Let us assume that the distance between the light source and wall is negligible. In this case, the wall itself behaves as a light emitting source. A camera is placed at  $m$  different distance values ( $D = \{d_1, d_2, \dots, d_m\}$ ) from the wall. For every distance value,  $n$  images are captured such that each image corresponds to one of the  $n$  voltage levels ( $V = \{v_1, v_2, \dots, v_n\}$ ). Let us represent every image by the corresponding distance-voltage value pair as  $I(d, v)$ . The total number of images is equal to  $mn$ .

For the first level of regression, every image is reduced down to a single value equal to mean image intensity  $i(d, v)$ . At this level, the model tries to learn the relationship between mean image intensity and distance for every voltage value. Since the wall is assumed to be behaving as a light source, the equation used for the first level of regression is based on the inverse-square law of light. The inverse-square law of light states that the intensity of illumination is inversely proportional to the square of distance from the source. For every voltage value  $v$ , the model tries to learn the coefficient  $x_v$  and intercept  $y_v$  as shown in Algorithm 1. Once the transfer functions relating intensity and distance have been obtained, the algorithm calculates the value of intensity multipliers corresponding to every distance value and returns an array of multipliers. Multipliers eliminate the effect of distance on intensity.

Once we have the multiplier array, we move on to the second regression level. Every image is flattened into a column vector such that cell  $k$  of the column represents mean intensity across row  $k$  of the image. Let us represent each column vector as  $IC(d, v)$ . All the column vectors are then stacked in a column called "IC" and we populate "dist" and "volt" columns with  $d$  and  $v$  values corresponding to every data point. Values of the IC column are normalized by their corresponding multipliers to make intensity readings independent of distance. The second regression model learns the transfer function connecting updated intensity values and voltage as shown in Algorithm 2, where  $h$  is a coefficient and  $q$  is the intercept. As an output of regression level 2, we obtain the final voltage prediction model. This is akin to removing the distance dimension from Figure 8.

In order to predict voltage using the model, image is passed on to the model along with the distance at which the image was captured.

**Table 1: Lighting Database Summary**

Bulb Type	Count	Wattage Range (W)	Price Range (\$/Unit)
CFL	16	9-32	3.49-5.89
Incandescent	10	60-200	1.29-6.99
Halogen	11	39-150	1.6-11.49
LED	36	4-23	2.89-17.99
Xenon	1	39	7.99

The image is flattened into a column vector and is operated upon to eliminate the effect of distance using the correct multiplier. The trained model then predicts the voltage vector associated with the input intensity vector.

## 7 IMPLEMENTATION

### 7.1 Equipment

We use IDS Vision’s UI-3480LE-M-GL monochrome camera, the One Plus 6 smartphone, and the Motorola G5 Plus smartphone. The One Plus 6 and Motorola G5 Plus were specifically selected for our experiments because the cameras in these phones support manual mode which is necessary for our frequency, phase, and voltage measurement techniques. Manual mode also allows us to keep the camera parameters consistent for all the experiments. The 16MP One Plus 6 camera is equipped with a F/1.7 physical aperture and CMOS Sony IMX519 sensor [6]. The 12MP Moto G5 Plus camera is equipped with a F/1.7 aperture and Sony IMX260 sensor [17, 22]. The IDS Vision camera possesses a 4.92MP CMOS sensor (MT9P031STM) and provides image resolution of 2560 x 1920 pixels. It can be controlled using IDS Vision’s freely available software suite. In addition to the imaging equipment, we used a B+W 62mm cross screen 4-point star filter for phase detection in outdoor scenes. Additionally, Powerstat’s 10A, 1.4kVA variable transformer was used to step voltage values up and down for voltage monitoring experiments.

### 7.2 Image Data Acquisition

For all the experiments, the phone cameras were operated at F2.0, ISO 800-1600, shutter speed 1/1000 – 1/800 (rolling image) and 1/60 (DC image). The vision camera was operated at F/1.4, Gain 9x, shutter speed 1/800 (rolling image) and 1/60 (DC image). We have developed an Android application and a script for the vision camera that automates the process of capturing rolling and DC images and it also stores camera’s GPS coordinates.

We captured images of a wall using cell phone cameras, extracted a column of pixels from each image, and applied a discrete Fourier transform to the extracted signal [25]. The frequency value corresponding to maximum signal energy was then selected as the spatial frequency of the image and was used to calculate the inter-row delay  $D$  as discussed in Section 4.

### 7.3 Lighting Database

Sheinin et al. [24, 25] developed a database of BRFs of around 30 bulbs for 230V/50Hz grids. To study and better understand the behavior of different light sources, we developed our own lighting database for 120V/60Hz grid systems. Our lighting database

contains BRFs of 81 different light bulbs from 10 different companies, and other information like actual power consumption, labeled wattage, illuminance (lux), manufacturer, price, and company name\*. Table 1 summarizes the spread of our lighting database. BRFs were sensed using SparkFun’s TEMT6000 light sensor and MSOX2024A oscilloscope. Every bulb was connected to the same power outlet in the lab and the distance between a bulb and the sensor was maintained constant at 40cm. BRF recording for every bulb was triggered on the rising edge at the zero-crossing of power supply voltage for maintaining consistency in database readings. BRFs of a few bulbs and the AC input waveform are shown in Figure 1. The recorded BRF data are used for a phase detection technique discussed in Section 5. The BRF data can also be used for on-the-fly bulb type detection and bulb identification in the future.

## 8 RESULTS AND EVALUATION

Here, we explore the capabilities and limits of imaging devices to measure grid parameters as discussed in Sections 4, 5, and 6.

### 8.1 Frequency Monitoring

We conducted frequency monitoring experiments in two countries - USA and India. The electric grid in the US operates at 120V/60Hz while in India it operates at 230V/50Hz. A set of 10 different bulbs per country was selected such that each set contained 3 CFL, 3 incandescent, 1 halogen, and 3 LED type bulbs. The criteria for selecting a specific bulb was: it has to be popular among and affordable by middle-income people in each respective country. Bulbs were then selected based on online reviews and inputs from local vendors in the US and India.

One bulb at a time was connected to the supply, and rolling and DC images of a wall illuminated by the bulb were captured using the imaging equipment. The vision camera was placed at a distance of 5ft from the wall and smartphone cameras were placed at 3ft from the wall. Every time a new bulb was brought in for the experiment, the supply frequency at the outlet was recorded using a multi-meter to be used as ground-truth data. We applied all the three frequency monitoring techniques discussed in Section 4 on the captured images. Calculated frequency was then compared with ground data to calculate mean absolute percentage errors (MAPE) associated with every method as shown in Table 2. All methods performed well but power spectral density (PSD) gave the most accurate results. Using the PSD technique we quantified the error in frequency measurement with varying distance between camera and the wall. We observed that beyond 5ft for Motorola and 6ft for OnePlus, the power of other frequency components was higher than the power of the nominal frequency component and so the detected frequency measurements were highly erroneous. Therefore, for all frequency and indoor phase detection experiments, smartphones were placed at a maximum distance of 5ft from the wall.

### 8.2 Phase Detection

#### 8.2.1 Phase Detection Indoors.

First, the phase connections of power outlets in our lab were mapped using an oscilloscope. Two outlets 240° apart in phase were then selected for the experiments. One outlet was assumed to be a reference outlet for all experiments.

\*Database will be publicly available at <http://traces.cs.umass.edu/index.php/Smart/Smart>

**Table 2: Errors in Frequency Detection**

	Peak Finding	PSD	Sine Fitting
Motorola G5 Plus	2.76%	1.98%	4.22%
One Plus 6	2.34%	1.75%	3.83%
IDS Vision Camera	1.55%	1.21%	2.60%

**Table 3: Errors in Phase Detection (Indoors)**

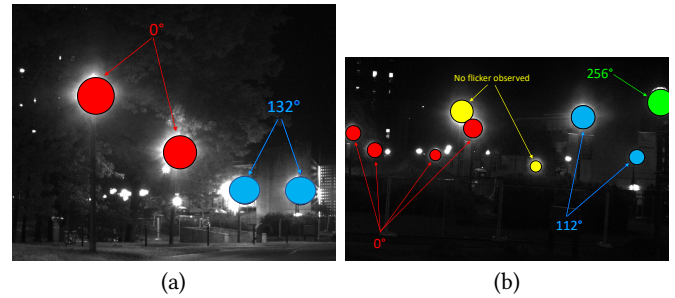
	Signal-Sine	Signal-BRF	Signal-Signal
Motorola G5 Plus	9.4%	5.0%	11.2%
One Plus 6	7.6%	4.1%	10.3%
IDS Vision Camera	6.5%	2.0%	7.8%

For a single experiment, we used two bulbs and connected them to the two power outlets. A rolling image and a DC image were then captured using the imaging equipment. We followed the same process of image normalization and flicker pattern extraction as discussed in Section 5. The wave patterns were then passed through two phase detection techniques, sine fitting and Signal-BRF fitting, to obtain the phase difference value. 10 experiments were conducted and each experiment involved a different pair of bulbs from our database. Table 3 displays a MAPE value for every technique. The Signal-BRF method performed significantly better than sine-fitting for images captured using smartphones and a vision camera. One major benefit of the sine-fitting technique is that it does not depend on the bulb type or its BRF, unlike the Signal-BRF technique.

We conducted one more study in which we ignored the BRFs and the bulb types. Using the same recorded images, we directly measured the time shift between the recorded signals and then calculated the phases. The results are provided in column Signal-Signal in Table 3. Results show that for cases when BRFs and bulb types are unknown, measuring phase shift between sine-fitted signals is better than measuring phase shift between the recorded signals. Nonetheless, the Signal-Signal method remains useful in cases when we cannot fit a sine-wave to the flicker signal and the BRFs are unknown. For example, flickering of some LEDs is not significant, making it difficult to fit a sine-wave to the signal.

### 8.2.2 Phase Detection Outdoors.

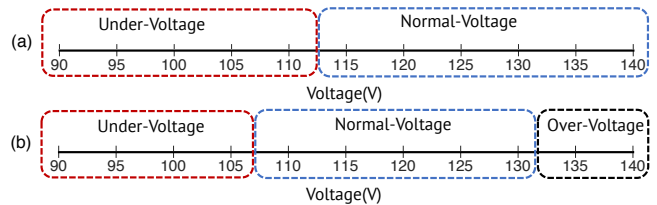
We selected two different outdoor scenes for phase detection experiments. Rolling and DC images for every scene were captured using two methods - defocusing the lens and using a 4-point star filter. Flicker wave patterns for every source were extracted as discussed in Section 5. We only applied Signal-Sine and Signal-Signal methods for phase calculations since we did not have BRFs of lamps in the outdoor scenes. Figure 9 displays the detected phase values for bulbs in the captured scene. For the outdoor scenes, the recorded flicker wave signals for distant bulbs were very noisy which rendered inference of any information nearly impossible. This calls for the use of more powerful lenses. Another observation from our outdoor experiments was that our two smartphone cameras do not have enough defocusing capability to be able to produce significant point spread functions of light sources and so the potential to use the defocusing technique with smartphones may be in question. This may be solved by attaching powerful external lenses to the phone camera.

**Figure 9: Phase detection for outdoor scenes captured using an IDS vision camera in a (a) street and (b) parking lot.****Table 4: Errors in Phase Detection (Emulated Outdoors) - Defocusing**

	Signal-Sine	Signal-BRF	Signal-Signal
Motorola G5 Plus	100%	99.7%	100%
One Plus 6	100%	98.9%	100%
IDS Vision Camera	7.9%	3.6%	8.1%

**Table 5: Errors in Phase Detection (Emulated Outdoors) - Star Filter**

	Signal-Sine	Signal-BRF	Signal-Signal
Motorola G5 Plus	12.7%	10.0%	16.5%
One Plus 6	10.8%	7.5%	11.6%
IDS Vision Camera	7.8%	3.1%	8.6%

**Figure 10: Discrete voltage value classification: (a) without bias correction and (b) with bias correction**

We did not possess ground truth data for the bulbs in outdoor scenes. In order to assess the effectiveness of phase detection for outdoor scenes and to verify our observations, we created a simple setup to emulate an outdoor scene in our lab with 3 lamps directly visible to the cameras with known types, BRFs, and phase connections of the bulbs involved. The complete phase detection experiment was repeated for three different positions of light sources in the room. Table 4 and Table 5 provide the evaluation results of both the flicker inducing methods in the form of MAPE. The star filter method demonstrated an overall better performance compared to camera defocusing.

## 8.3 Voltage Monitoring

We selected a range of 5 different bulbs for our voltage monitoring experiments - 2 CFL, 2 incandescent, and 1 LED. For the data collection process, one bulb at a time was connected to an outlet via a voltage transformer and a camera was used to capture a wall illuminated by the bulb. The camera was placed at 5 different distances from the wall - 5ft, 6ft, 7ft, 9ft, and 11ft. At every stop,

**Table 6: Test Case Voltage Prediction Results**

Device	Bulb	MAE	RMSE	MAPE (%)
One Plus 6	CFL1	13.60	15.76	12.16
	CFL2	12.56	15.80	11.20
	Incan1	13.54	15.67	12.12
	Incan2	13.52	15.98	12.09
	LED1	13.68	14.56	12.17
Vision Cam	CFL1	9.37	11.68	8.33
	CFL2	10.01	12.65	9.18
	Incan1	6.42	8.27	5.93
	Incan2	9.31	12.28	8.29
	LED1	11.46	13.12	10.48

images were captured for 11 different AC voltage settings ranging from 90V to 140V in steps of 5V. Multiplier arrays corresponding to every bulb were obtained using the first regression level. K-fold cross validation was then employed to split data into training and testing sets for each bulb. Regression level 2 model i.e. the voltage prediction model was trained using the training data-set. The test case voltage prediction error results - mean absolute error (MAE), root mean square error (RMSE), mean absolute percentage error (MAPE) values have been presented in Table 6. As shown in Table 6, the MAPE range of our models is 6 to 12.5% which is sufficient to detect a brownout, and it can be seen that the vision camera gives relatively better prediction results.

It is not feasible to have a model for every bulb, and so we studied the behavior of trained models when they encounter a bulb with a similar BRF but not exactly the one for which they were trained. Corresponding to every trained model, we selected one held out bulb with a similar BRF. Held out bulbs were supplied with 90-140V AC supply in steps of 5V, and corresponding images were recorded from a distance of 9ft. Held out bulb image data was then passed onto corresponding trained models for prediction. It was observed that the prediction error for voltage range 105-130V was much lower compared to that of a wider range of 90-140V. This indicates that the trained models' performance deteriorates at the edges of our voltage range. The model can effectively be used to detect brownouts or under-voltage events. According to the utility PG&E's national steady state voltage regulation standards [20], the utilization level voltage can vary from -13% to +6% of nominal 120V, i.e., in the range 104.4V to 127.2V. Let us label voltage predicted by CFL1 model for the held out case as under-voltage if it is less than 105V, normal-voltage if it is between 105 and 130V, and over-voltage beyond 130V. As shown in Figure 10(a), the model was able to classify brown-outs with some error but not over-voltage events. If we correct for a bias in predicted voltages, all the events were perfectly classified, as shown in Figure 10(b).

## 9 DISCUSSION

### 9.1 Potential Applications

Smartphones are pervasive and their ability to passively measure grid parameters could provide us with a low-cost part-time monitoring system at grid-edges, as opposed to smart meters [9]. Attaching the vision devices to utility vehicles or public transport vehicles could help monitor streets and houses in the area. Acquired data can then be used to detect and pin-point regions with poor power quality. Voltage problems associated with a specific group of houses can

**Table 7: Held Out Case Voltage Prediction Results**

Device	Bulb	MAE	RMSE	MAPE (%) (90-140V)	MAPE (%) (105-130V)
One Plus 6	CFL1	19.61	20.77	16.34	9.02
	CFL2	18.63	19.34	14.42	11.78
	Incan1	21.59	23.75	19.59	13.66
	Incan2	17.4	18.21	15.93	10.74
	LED1	19.48	21.93	16.29	11.38
Vision Cam	CFL1	12.10	15.07	10.99	8.09
	CFL2	14.16	16.66	11.36	9.90
	Incan1	37.20	38.54	32.17	15.39
	Incan2	15.63	17.45	14.21	9.31
	LED1	19.15	22.35	14.93	9.04

usually be tracked down to the distribution transformer supplying electricity to their homes, and can help utility personnel conduct predictive maintenance of their system for ensuring reliability.

As an example application, unreliable electricity supply in sub-Saharan Africa causes many customers to purchase backup diesel generators. Farquharson et al. [7] show that backup diesel power is very expensive compared to grid electricity and is also a significant source of pollution. Frequency and phase detection techniques proposed in this paper can be used to detect and count backup generators in a region which can help inform better decision making in the systems planning process.

A balanced three-phase power system can become unstable if there is a significant difference in the energy consumption on different phases. Imbalance can increase stress on various distribution grid components and cause faulty operation of protection equipment [16]. To keep a system balanced and stable, it is crucial to maintain data on phase connections of customers, which our system can do. Customer phase information can also be of great value for balancing the systems with increasing renewable integration and for successful incorporation of demand response programs [16]. Buevich et al. [5] demonstrated that upstream supply data and downstream consumption data cannot only be used to calculate microgrid losses but also to estimate non-technical losses. Incorporating data acquired using our phase detection technique could provide more granular phase-level insights into grid loss measurements which could potentially be used to detect electricity theft.

### 9.2 Limitations and Deployment Challenges

Since the photos taken at night contain noise, it becomes difficult to record the useful flicker information beyond a certain distance from the scene. Using our current techniques, this limits reach to 3-5ft from the scene if using smartphone cameras. Better cameras might help in improving the distance range for capturing reliable readings but it is yet to be explored. Post-processing software of different phone cameras play a major role in rendering an image and can possibly affect our measurements but we have not yet studied its effect in detail. Since sensors in cameras differ, changing a vision device can affect voltage prediction results. In such a case, one will have to develop completely new models by acquiring data using the new device. Also, not all LEDs flicker or have a sinusoidal waveform, so we will not be able to estimate source frequency from the flicker frequency. Our phase and frequency detection techniques will fail if an LED behaves as if operating on a DC supply. Additionally, in all

the experiments, we have not taken into consideration the aspect that some bulbs glow dimmer with age, which can incorrectly be interpreted as a brown-out condition. Another major deployment challenge is capturing stable images on-the-fly. Ambient conditions affect the quality of recorded information and requires automatic adjustment of ISO, shutter speed, and aperture within acceptable limits. Different scenes may demand a different set of lenses for the vision devices.

### 9.3 Future Work

We plan on conducting more *in situ* experiments to better understand the involved scene complexities and to refine our sensing methods. Imaging devices run on batteries and so it is necessary to understand the maximum time for which a fully charged vision device can capture images. Another way forward will be to study the improvement/deterioration of measurements taken using phone cameras with clip-on external lenses. Instead of having one voltage prediction model per bulb, we plan to reduce redundancy by developing a universal model that can be used to predict voltage across any AC powered source. One possible method of building a model can be through convolutional neural networks. A bulb identification algorithm, similar to the one developed by Yin et al. [27], will be developed to facilitate phase detection techniques that require knowledge of bulb type and BRF. One major ongoing aspect of this project is grid mapping. For grid mapping, we estimate GPS coordinates of a light source using GPS coordinates of our phone and features from images; then, we can localize the detected light sources for mapping. We are using tools like Simultaneous Localization and Mapping (SLAM) to achieve accurate localization. None of the techniques discussed in this paper can be applied towards wide-area scene monitoring. Our new direction will be to devise and demonstrate a technique using principles provided in [25] and [3] to detect frequency and phases in wide-area scenes using burst image capture. Additionally, burst capture of a scene at a high frame rate could possibly allow us to conduct more nuanced analysis of local power consumption.

## 10 CONCLUSION

We have demonstrated *GridInSight*, a set of techniques for measuring electricity grid parameters – frequency, phase, and voltage – using only images gathered with commodity cameras. Our results show errors of 1-2%, 2-5%, and 3-10% for measuring frequency, phase indoors, and phase outdoors, respectively, using a mix of smartphone and a machine vision camera. Further, we develop an entirely novel technique and show an error of 8-15% for measuring voltage on a lightbulb that our system had not seen previously. We believe these results herald a new capability to visually measure electricity grids, enabling new applications as diverse as backup generator mapping, phase map correction, and roaming power quality monitoring. We believe that *GridInSight* can contribute to better and more diverse measurement of electricity grids that will lead to more reliable and plentiful electricity everywhere.

## REFERENCES

- [1] O. Ait-Aider, A. Bartoli, and N. Andreff. 2007. Kinematics from Lines in a Single Rolling Shutter Image. In *2007 IEEE Conference on Computer Vision and Pattern Recognition*.
- [2] M. Albu, S. Mihai, and C. Stanescu. 2016. Syncretic Use of Smart Meters for Power Quality Monitoring in Emerging Networks. In *IEEE Transactions on Smart Grid*.
- [3] Federica B. Bianco, Steven E. Koonin, Charlie Mydlarz, and Mohit S. Sharma. 2016. Hypertemporal Imaging of NYC Grid Dynamics: Short Paper. In *Proceedings of the 3rd ACM International Conference on Systems for Energy-Efficient Built Environments (BuildSys '16)*, 61–64. <http://doi.acm.org/10.1145/2993422.2993570>
- [4] J. Breda and J. Taneja. 2018. Fancy That: Measuring Electricity Grid Voltage Using a Phone and a Fan. In *1st ACM SIGCAS Conference on Computing and Sustainable Societies*.
- [5] M. Buevich, X. Zhang, O. Shih, D. Schnitzer, T. Escalada, A. Jacquiau-Chamski, J. Thacker, and A. Rowe. 2016. Microgrid Losses: When the Whole Is Greater Than the Sum of Its Parts. In *2016 ACM/IEEE 7th International Conference on Cyber-Physical Systems (ICCCPS)*, 1–10.
- [6] Edgar Cervantes. [n.d.]. OnePlus 6 camera review. Retrieved June 6, 2019 from <https://www.androidauthority.com/oneplus-6-camera-review-885975/>
- [7] D. Farquharson, P. Jaramillo, and C. Samaras. 2018. Sustainability implications of electricity outages in sub-Saharan Africa. *Nature Sustainability* 1, 10 (October 2018).
- [8] R. Garg, A. Varna, A. Hajj-Ahmad, and M. Wu. 2013. Seeing ENF: Power-Signature-Based Timestamp for Digital Multimedia via Optical Sensing and Signal Processing. *IEEE TRANSACTIONS ON INFORMATION FORENSICS AND SECURITY* 8, 9 (September 2013).
- [9] V. Gripp, F. Bianco, A. Yoshino, E. Gonzalez, T. Dam, and X. Gao. [n.d.]. Hypertemporal Imaging: An alternative technology to monitor grid dynamics. Retrieved June 26, 2019 from <https://www.authorea.com/users/106918/articles/162707-hypertemporal-imaging-an-alternative-technology-to-monitor-grid-dynamics>
- [10] J. Gu, Y. Hiomi, T. Mitsunaga, and S. Nayar. 2010. Coded Rolling Shutter Photography: Flexible Space-Time Sampling. In *2010 IEEE International Conference on Computational Photography (ICCP)*.
- [11] Monson H. Hayes. 1996. *Statistical Digital Signal Processing and Modeling* (1st ed.). John Wiley & Sons, Inc., New York, NY, USA.
- [12] K. Jo, M. Gupta, and S. Nayar. 2016. DisCo: Display-Camera Communication Using Rolling Shutter Sensors. *ACM Transactions on Graphics* 35, 5 (July 2016).
- [13] J. Jose Gonzalez de la Rosa and A. Moreno-Munoz. 2010. A web-based distributed measurement system for electrical Power Quality monitoring. In *2010 IEEE Sensors Applications Symposium*.
- [14] R. Fadel Khelifa and Khaled Jelassi. 2017. An energy and power quality monitoring system of a power distribution. In *2016 International Conference on Electrical Sciences and Technologies in Maghreb (CISTEM)*.
- [15] C. Liang, L. Chang, and H. Chen. 2008. Analysis and Compensation of Rolling Shutter Effect. *IEEE TRANSACTIONS ON IMAGE PROCESSING* 17, 8 (August 2008).
- [16] M. Sadegh Modarresi, T. Huang, H. Ming, and L. Xie. 2017. Robust phase detection in distribution systems. In *2017 IEEE Texas Power and Energy Conference*.
- [17] Motorola. [n.d.]. Motorola G5 Plus Full Specifications. Retrieved June 6, 2019 from <https://www.motorola.com/us/products/moto-g-plus>
- [18] M. Music, A. Bosovic, N. Hasanspahic, S. Avdakovic, and E. Becirovic. 2013. Integrated power quality monitoring system and the benefits of integrating smart meters. In *2013 International Conference-Workshop Compatibility And Power Electronics*.
- [19] E. Palacios-Garcia, E. Rodriguez-Diaz, A. Anvari-Moghaddam, M. Savaghebi, J. Vasquez, J. Guerrero, and A. Moreno-Munoz. 2017. Using smart meters data for energy management operations and power quality monitoring in a microgrid. In *2017 IEEE 26th International Symposium on Industrial Electronics*.
- [20] PGE. 1999. Voltage Tolerance. Retrieved June 3, 2019 from [https://www.pge.com/includes/docs/pdfs/mybusiness/customerservice/energystatus/powerquality/voltage\\_tolerance.pdf](https://www.pge.com/includes/docs/pdfs/mybusiness/customerservice/energystatus/powerquality/voltage_tolerance.pdf)
- [21] E. Ringaby and P. Forssen. 2011. Efficient Video Rectification and Stabilisation for Cell Phones. *International Journal of Computer Vision* 96, 3 (June 2011), 335–352.
- [22] Tim Schiesser. [n.d.]. Motorola Moto G5 and G5 Plus Review: Camera. Retrieved June 6, 2019 from <https://www.techspot.com/review/1402-motorola-moto-g5/page5.html>
- [23] S.K. Shah, A. Hellany, M. Nagrial, and J. Rizk. 2015. Review of Power Quality Monitoring Web-based Techniques. In *2015 Australasian Universities Power Engineering Conference*.
- [24] M. Sheinin, Y. Schechner, and K. Kutulakos. 2017. Computational Imaging on the Electric Grid. In *The IEEE Conference on Computer Vision and Pattern Recognition (CVPR)*.
- [25] M. Sheinin, Y. Schechner, and K. Kutulakos. 2018. Rolling shutter imaging on the electric grid. In *2018 IEEE International Conference on Computational Photography (ICCP)*. IEEE, 1–12.
- [26] H. Su, A. Hajj-Ahmad, R. Garg, and M. Wu. 2017. EXPLOITING ROLLING SHUTTER FOR ENF SIGNAL EXTRACTION FROM VIDEO. In *2014 International Conference on Image Processing*.
- [27] S. Yin, T. Oliveira, and A. Murthy. 2017. Automated Lamp-Type Identification for City-Wide Outdoor Lighting Infrastructures. In *Proceedings of the 18th International Workshop on Mobile Computing Systems and Applications*.
- [28] M. Zhou. 2016. Vibration Extraction Using Rolling Shutter Cameras. <https://pdfs.semanticscholar.org/beba/4d8fd35a264a082416fc06b4dba144eb4307.pdf>